9. The cell suspension was gently pipetted up and down to resuspend cells on the bottom of the centrifuge tube, and the cell density was counted with the use of flow cytometry (Coulter EPICS™ XL, Beckman-Coulter Co.).

Cell Permeation

KUSA-A1 cells and H-1/A cells were inserted into the centrifugation tube containing DMEM medium. Each cell density was adjusted to be 50,000 cells/mL by the addition of DMEM medium. The single- or mixed-cell solution of 6 mL containing KUSA-A1 cells and/or H-1/A cells was permeated through the membranes with the permeation apparatus described in the previous study.[14] The diameter of the membrane was 25 mm and filtration rate was 1 mL/min. The number of each cell of KUSA-A1 cells and H-1/A cells in the permeate and feed solutions (N_p and N_f, respectively) was counted from the flow-cytometry measurements.

The permeation ratio is defined as

$$\text{permeation ratio } (\%) = (N_p/N_f) \times 100. \quad (1)$$

After the cell filtration, the membrane was upside down inside the membrane holder, and 0.5-wt % HSA solution of 6 mL was permeated through the membrane with the use of the same membrane and the apparatus at filtration speed of 1 mL/min to remove the attached cells on the membrane and to collect them in the HSA solution. The recovery ratio is defined as

$$\text{recovery ratio } (\%) = (N_r/N_f) \times 100, \quad (2)$$

where N_r is the number of cells in the permeate solution after the permeation of HSA solution. The filtration experiments were performed at 25±0.5°C.

The membranes used in the cell filtration were unmodified PU membranes, surface-modified PU membranes, nylon-net filters, nonwoven fabrics, and silk screens. The permeation experiments of cells were performed on each membrane with four independent membranes.

Flow-Cytometric Analysis of Cells

The size and shape of KUSA-A1 cells and H-1/A cells were analyzed from forward light scattering and side light scattering of laser beam (Ar laser, 488 nm) by flow cytometry. The number of KUSA-A1 cells and H-1/A cells in the feed and permeate solutions was analyzed from flow-cytometric scattergrams of KUSA-A1 cells and H-1/A cells in the fluorescent intensity at 575 and 525 nm.

SEM Analysis of Cells on the Membranes

After permeation of suspended cell solution through the membranes, the membranes were rinsed with saline. Consequently, the membranes were treated with 3-wt % glutaraldehyde in saline for 2 days at 4°C. The samples were washed with saline, subjected to a drying process by being passed through a series of graded-alcohol–saline solutions (0, 25, 50, 75, and 100%) and dried in a vacuum for 10 h at room temperature.[20] The dried membranes were gold coated and examined with the use of a JSM-5200 scanning electron microscope (SEM, JEOL, Ltd.).

RESULTS AND DISCUSSION

Flow-Cytometric Analysis of Cells

KUSA-A1 osteoblasts and H-1/A preadipocytes, two mesenchymal cell lines, were incubated with fluorescent probes (Cell Tracker Orange™ and Cell Tracker Green™, respectively) to allow their independent detection before and after permeation through porous polymeric membranes. The numbers of KUSA-A1 and H-1/A cells in the mixed cell solution were determined from flow-cytometric scattergrams at 575 nm for KUSA-A1 cells and 525 nm for H-1/A cells. These values are close to those of phycoerythrin (PE) and fluorescein isothiocyanate (FITC), which are used for conventional cell-counting of specific cells.[21] Figure 1(a) shows the flow-cytometric scattergrams for the KUSA-A1 and H-1/A cells. The fluorescence intensities at 525 and 575 nm for the two cell types were significantly different. The forward and side light scattering intensities, shown in Figure 1(b), indicate that both cell types have a broad size distribution, although KUSA-A1 cells are mostly smaller than H-1/A cells. Furthermore, the flow-cytometric scattergrams of KUSA-A1 cells and H-1/A cells (forward light scattering intensity vs. side light scattering intensity and fluorescence intensity at 525 nm vs. 575 nm) were found to be identical in single- and mixed-cell solutions (data not shown). Thus, cell aggregates did not appear to be formed when KUSA-A1 cells and H-1/A cells were mixed together in DMEM medium.

Cell Separation Through PU Membranes

The differences in the cell sizes and shapes suggested that KUSA-A1 and H-1/A cells can be separated by using porous polymeric membranes. This possibility was examined with the use of a variety of membrane types. Figure 2 shows an SEM image of the surface of the porous polymeric membranes tested in this study. A regular screen pore morphology was found on the surface of nylon-net filters [Figure 2(b)] and silk screens [Figure 2(e,f)], whereas a specific pore morphology was not found on the surface of nonwoven fabrics [Figure 2(c,d)]. Furthermore, a deformed open pore structure was found on the surface of the PU membranes used in this study [Figure 2(a)].

The permeation of cells through PU and surface-modified PU membranes was investigated first, because a previous study showed that hematopoietic stem cells can be recovered from peripheral blood with the use of surface-modified PU (PU-COOH) membranes.[14] The permeation of KUSA-A1 cells, H-1/A cells, and a mixture of the two cell types through PU and surface-modified PU membranes (pore size = 12 μm) at 25°C was examined. Figure 3(a) shows the permeation ratio through the membranes with a suspension of a single cell type (50,000 cells/mL) used as the feed solution, and Figure 4(a) shows the results obtained when the feed solution was a mixture of the two cell types. A relatively low (< 6%) permeation ratio through PU and surface-modified PU membranes was found with either a single-cell solution or a mixed-cell solution. Because open pore volume of the

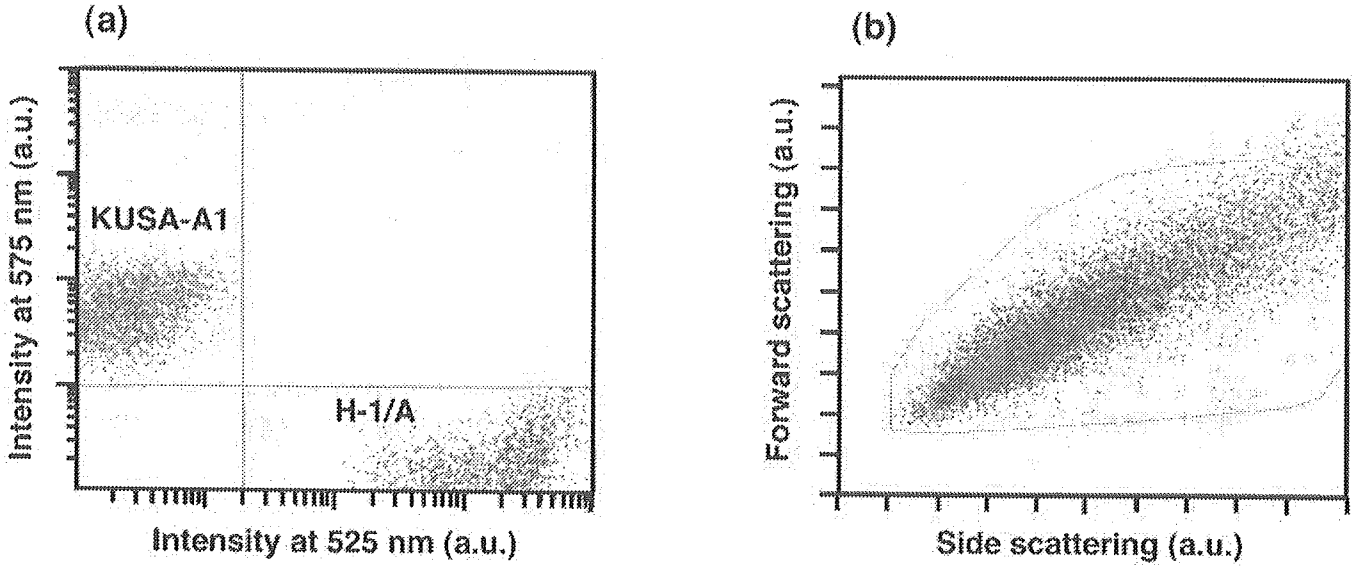

Figure 1. Flow-cytometric scattergrams of mixed solution of KUSA-A1 cells (orange dots) and H-1/A cells (green dots), each having a cell density of 50,000 cells/mL in the fluorescent intensity at 575 nm and 525 nm (a) and in the light intensity of forward scattering and side scattering (b). [Color figure can be viewed in the online issue, which is available at www.interscience.wiley.com.]

membrane interior in PU and surface-modified PU membranes is calculated as 0.506 mL (i.e., 1.25 cm × 1.25 cm × 3.14 × 0.12 cm × 0.86) and total cell volume permeated through the membranes is approximately calculated as 3.375×10^{-4} mL in a mixed-cell solution [i.e., 6 mL × 50,000 cells/mL × 2 × (7.5×10^{-4} cm × 7.5×10^{-4} cm ×

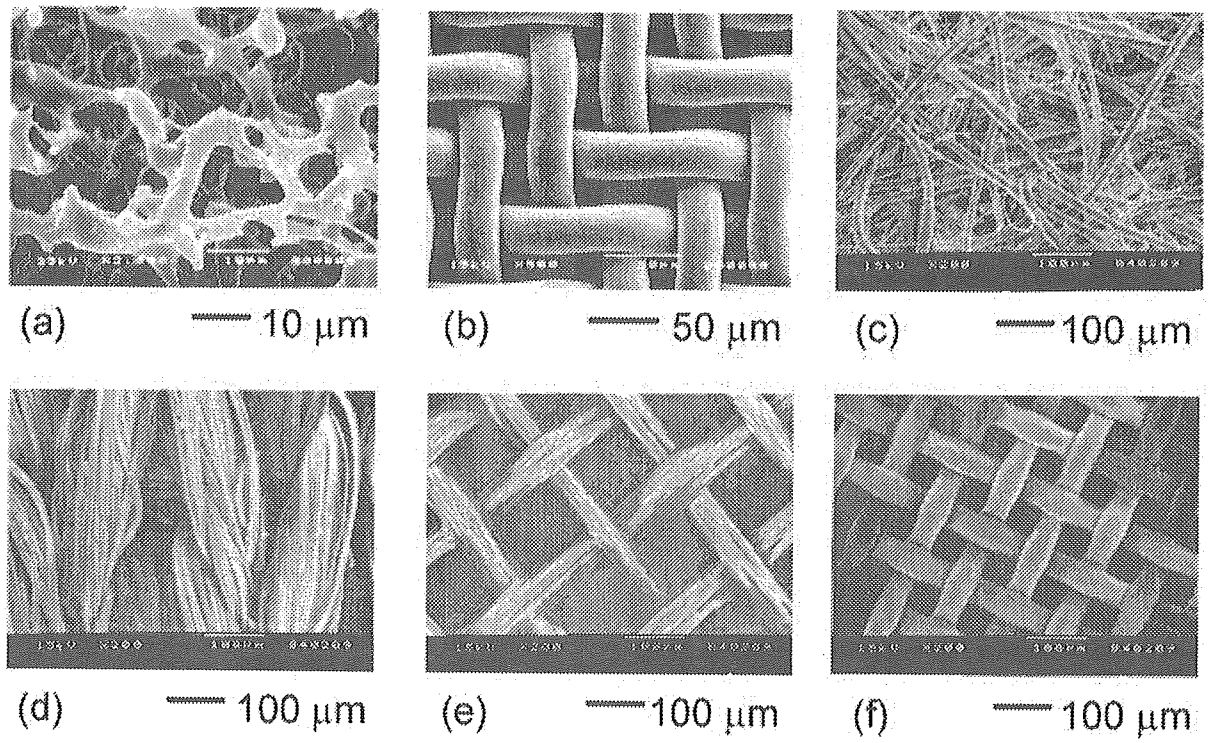

Figure 2. Scanning electron micrographs of the membrane surfaces of (a) unmodified PU membranes, (b) nylon-net filter, (c) nonwoven fabrics made of acrylonitrile, (d) nylon + polyester, (e) silk screens made of silk mesh size 150), and (f) silk screens made of Tetron™ (mesh size 250).

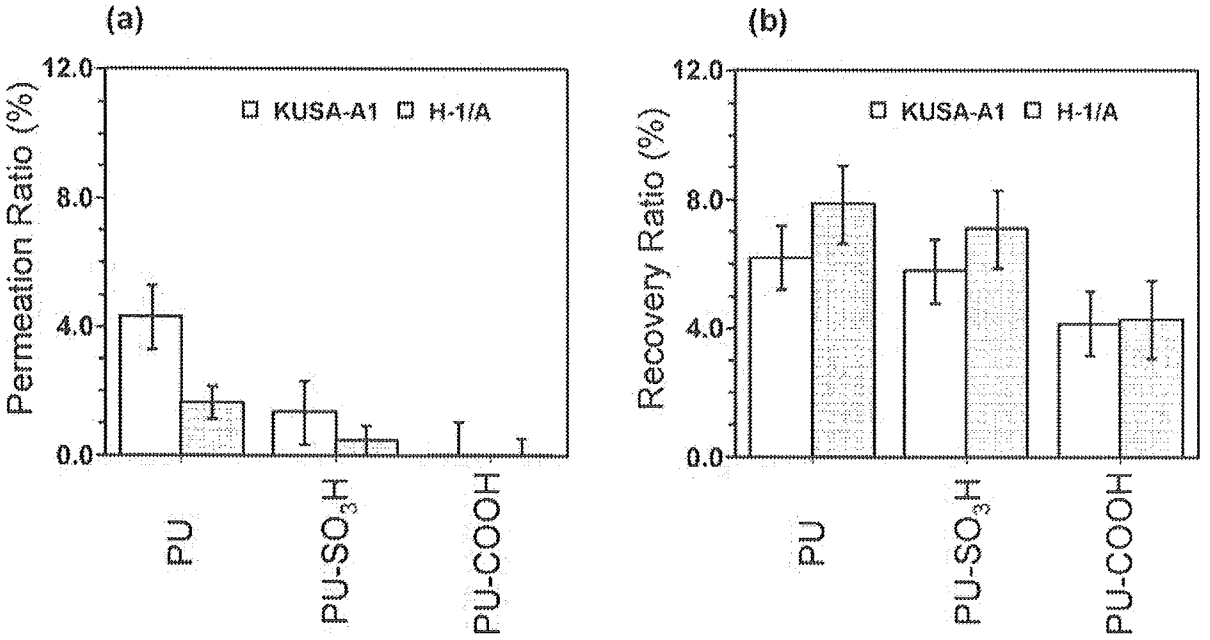

Figure 3. Permeation ratio (a) and recovery ratio (b) of KUSA-A1 cells and H-1/A cells through PU, PU-SO_3H, and PU-COOH membranes after permeation of single-cell solution at the cell density of 50,000 cells/mL and 25°C. Data are expressed as the means ± standard deviation of four independent measurements.

7.5×10^{-4} cm × 4/3)] in this study, the low permeation ratio is not due to the overloading of the cells permeated through the membranes. The low permeation ratio through PU and surface-modified PU membranes is due to high degree of cell adhesion on the membranes and a complicated pore structure of the membranes.

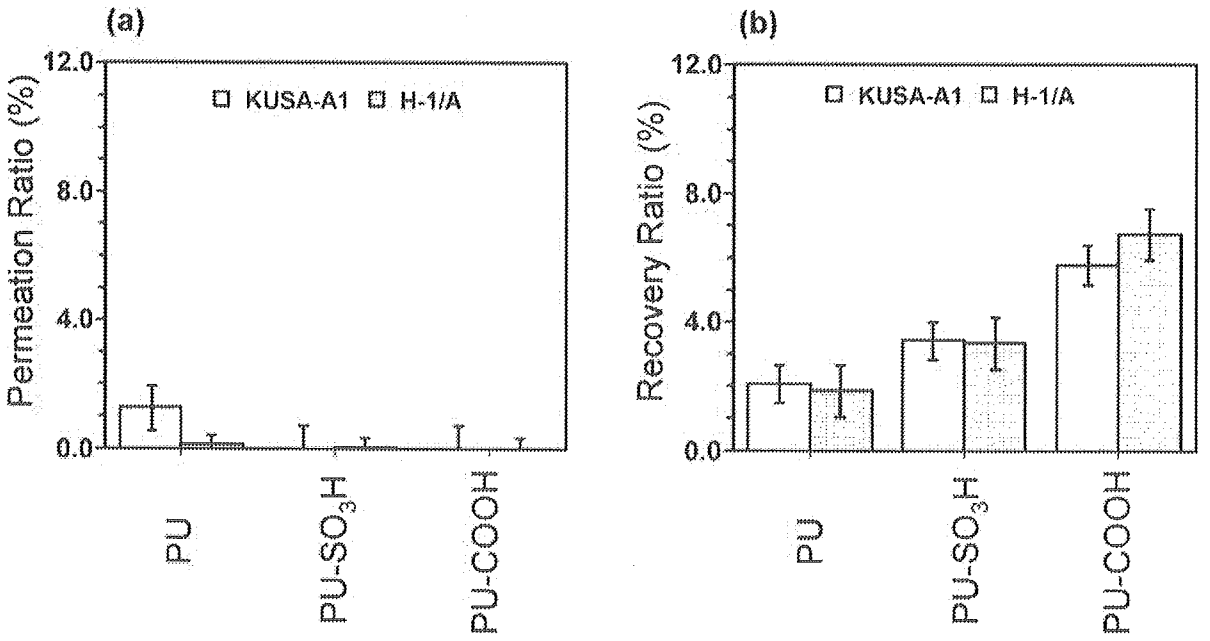

Figure 4. (a) Permeation ratio and (b) recovery ratio of KUSA-A1 cells and H-1/A cells through PU, PU-SO_3H, and PU-COOH membranes after permeation of mixed-cell solution at a cell density of 50,000 cells/mL each and 25°C. Data are expressed as the means ± standard deviation of four independent measurements.

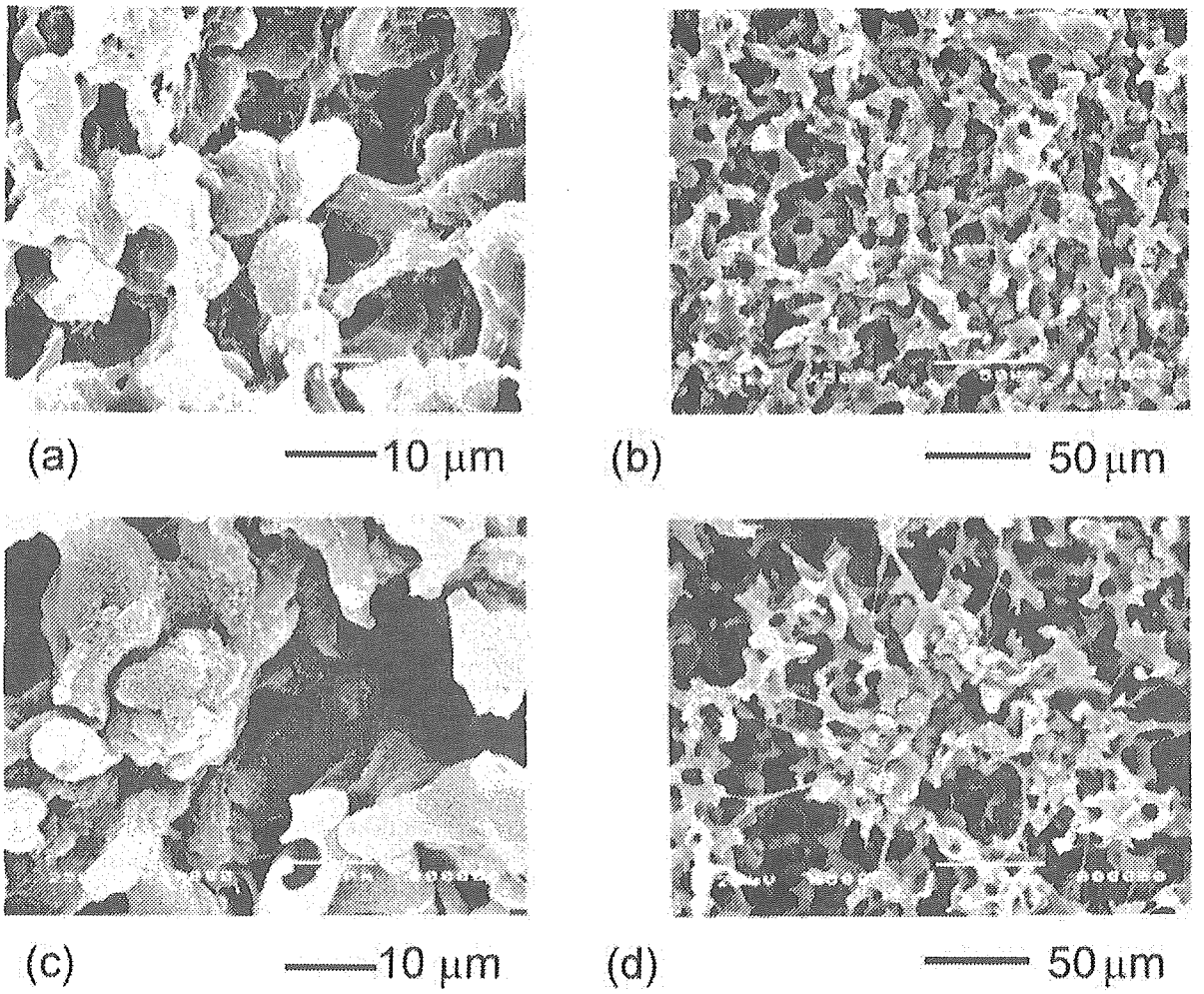

Figure 5. Scanning electron micrograph of membrane surface of unmodified PU membranes after permeation of KUSA-A1 cells (a), (b) or H-1/A cells (c), (d) at the cell density of each 50,000 cells/mL and 25°C.

The permeation ratio of both KUSA-A1 and H-1/A cells through PU membranes was found to be higher than that through PU-SO_3H and PU-COOH membranes. The surface modification of PU-SO_3H and PU-COOH membranes may cause the decreased pore size of the surface-modified membranes compared to the unmodified PU membranes. The permeation ratio when the feed solution contained a single cell type was found to be higher than the permeation ratio when it was a mixed-cell solution through PU and surface-modified PU membranes. Although FACS analysis suggested that coagulation or interaction does not occur between KUSA-A1 and H-1/A cells (data not shown), some coagulation or interaction between KUSA-A1 and H-1/A cells that was not detected from FACS analysis might lead to a decrease of the permeation ratio in the mixed-cell solution compared to the permeation ratio in the single-cell solution. It was also found that the permeation ratio for KUSA-A1 cells was higher than for H-1/A cells, which is consistent with the relatively smaller size of KUSA-A1 cells, as found in Figure 1(b).

Figure 5 shows a SEM image of the PU membrane surface after the permeation of KUSA-A1 or H-1/A cells. There was extensive adhesion of the KUSA-A1 and H-1/A cells to the membrane surface. The high adhesiveness of the cells may explain their low permeation ratios through the PU membranes. SEM images also revealed that the size of KUSA-A1 cells was similar to that of H-1/A cells (approximately 10 to 15 μm in diameter).

Next the effect of passing a HSA solution through the membranes following permeation of the single-cell or mixed-cell solutions was examined. Figures 3(b) and 4(b) show that the recovery ratio of KUSA-A1 and H-1/A cells following this treatment was higher than the permeation ratio. However, the recovery ratio was still below 10% through any of the PU membranes. Slightly higher recovery ratio through the PU and PU-SO_3H membranes in a mixed feed solution was found when compared to that in a single-cell type. On the other hand, no significant difference in recovery ratio was found between feed solutions containing a single cell type or a mixture of cell types through PU-COOH membranes.

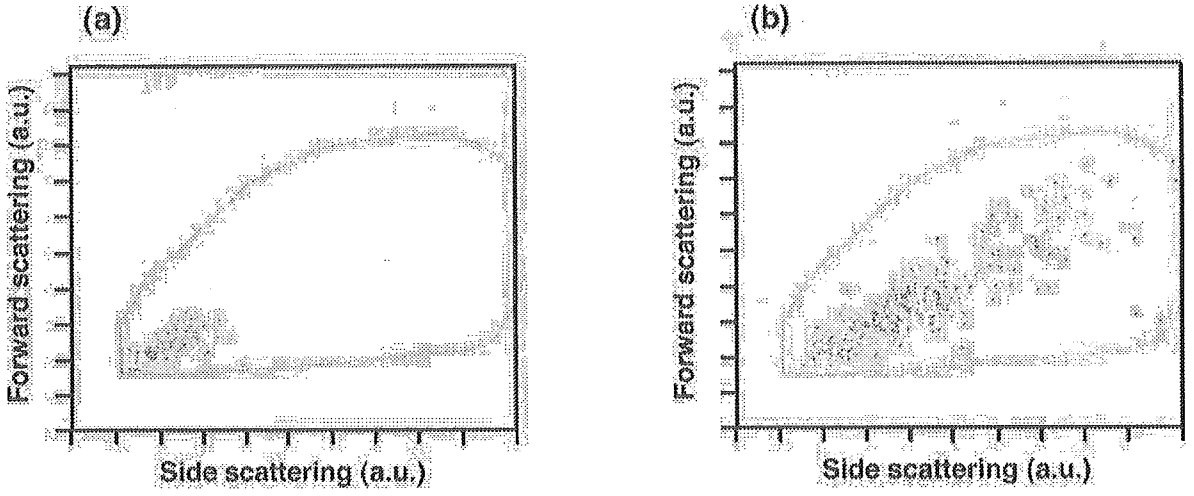

Figure 6. Flow-cytometric scattergrams of KUSA-A1 cells (orange dots) and H-1/A cells (green dots) in the relationship between forward light scattering intensity and side light scattering intensity in the permeate solution after permeation of mixed cells of KUSA-A1 cells (orange dots) and H-1/A cells (green dots) through the PU membranes at (a) the cell density of each 50,000 cells/mL, and (b) following subsequent permeation of HSA solution. [Color figure can be viewed in the online issue, which is available at www.interscience.wiley.com.]

Next the flow-cytometric analysis of the permeate solution of KUSA-A1 and H-1/A cells and also that of the recovery solution following filtration through PU membranes were examined. Figure 6(a) shows the forward versus side light scattering intensity in the permeate solution after permeation of the cells through PU membranes. Both smaller-sized KUSA-A1 and H-1/A cells passed through the PU membranes. Therefore, KUSA-A1 cells have a higher permeation ratio than H-1/A cells, because KUSA-A1 cells are typically smaller than H-1/A cells (see Figure 1).

Figure 6(b) shows the results of recovery solution following subsequent permeation of HSA solution. The pattern of the scattergram in the recovery solution [Figure 6(b)] was identical to that of the feed solution [Figure 1(b)], even though the numbers of both KUSA-A1 cells and H-1/A cells were significantly lower in the recovery solution. Thus, there is not a significant separation of KUSA-A1 and H-1/A cells in the recovery solution following permeation with HSA solution.

Cell Separation Through Various Porous Membranes

The separation of KUSA-A1 and H-1/A cells by several porous membranes, including uncoated nylon-net filters, fibronectin- or collagen-coated nylon-net filters, nonwoven fabrics made of acrylonitrile or a combination of nylon and polyester, silk screen No. 150 made of silk or Tetron™, and silk screen No. 250 made of Tetron™ were also examined. Figure 7 shows the permeation ratio through these membranes with the use of a feed solution containing a mixture of KUSA-A1 and H-1/A cells. With the use of the nylon-net filter and fibronectin-coated nylon-net filter, the permeation ratio for KUSA-A1 cells was higher than for H-1/A cells.

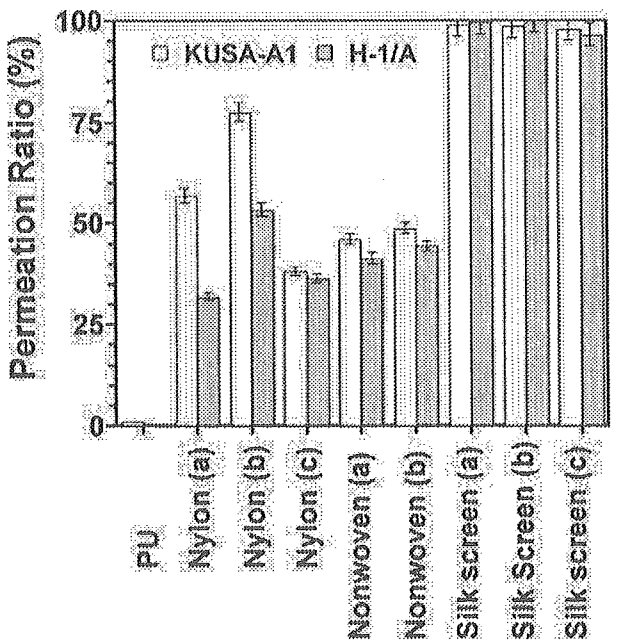

Figure 7. Permeation ratio of KUSA-A1 cells and H-1/A cells through PU, nylon-net filter [nylon (a)], nylon-net filter coated with fibronectin [nylon (b)] and collagen [nylon (c)], nonwoven fabrics made of acrylonitrile [nonwoven (a)], nylon and polyester [nonwoven (b)], and silk screens made of silk [silk screen (a), mesh size 150] and Tetron™ [silk screen (b), mesh size 150 and silk screen (c), mesh size 250] after permeation of mixed-cell solution at the cell density of 50,000 cells/mL and 25°C. Data are expressed as the means ± standard deviation of four independent measurements.

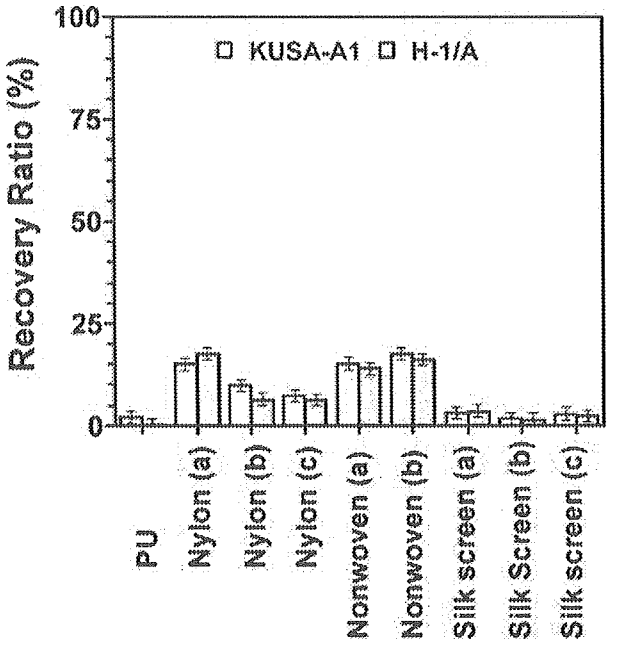

Figure 8. Recovery ratio of KUSA-A1 cells and H-1/A cells through PU, nylon-net filter [nylon (a)], nylon-net filter coated with fibronectin [nylon (b)] and collagen [nylon (c)], nonwoven fabrics made of acrylonitrile [nonwoven (a)], nylon and polyester [nonwoven (b)], and silk screens made of silk [silk screen (a), mesh size 150] and Tetron™ [silk screen (b), mesh size 150 and silk screen (c), mesh size 250] after permeation of mixed-cell solution at the cell density of 50,000 cells/mL and 25°C. Data are expressed as the means ± standard deviation of four independent measurements.

This is mainly due to the smaller cell size of the KUSA-A1 cells as detected in the forward and side light scattering intensities shown in [Figure 1(b)]. In addition, a high cell permeation ratio was also found with the use of silk screens made of silk or Tetron™. This was because silk screens have a larger pore size than the nylon-net filter and PU membranes (see Figure 2). A relatively good separation factor for permeation (α_P), defined as the relative permeation ratio of KUSA-A1 cells divided by that of H-1/A cells, was obtained when the mixed-cell solution was passed through the nylon-net filter (α_P = 1.8) or fibronectin-coated nylon-net filter (α_P = 1.5) membranes, whereas a separation was not obtained when the nonwoven fabrics or silk screens were used. Overall, the results suggest that the pore size of nylon-net filter was optimal for producing a sieving effect.

The effect of passing the HSA solution through the porous polymeric membranes after permeation of the cell mixture was also assessed. As shown in Figure 8, the recovery ratio of both KUSA-A1 and H-1/A cells was relatively low (< 20%) for all of the membranes. This is caused by the high adhesiveness of the mesenchymal cells and their high permeation ratio. Analysis of the recovery solution shows that there was no effective separation of KUSA-A1 and H-1/A cells. This is probably due to the fact that the KUSA-A1 and H-1/A cells are both mesenchymal cells and have similar characteristics (i.e., adhesiveness).

CONCLUSIONS

These results show that a separation of cells with similar characteristics, such as different types of mesenchymal cells (i.e., osteoblasts and preadipocytes) can be obtained in the permeate solution, but not in the recovery solution following membrane filtration. The main factor in this separation is the sieving effect of cells through the porous membranes. Therefore, prior to separation, flow cytometry should be carried out to confirm that the cells to be separated have different sizes. Separation factor, (α_P = 1.8) and a high permeation ratio was achieved when a mixed-cell solution was passed through a nylon-net filter with an 11-μm poor size, whereas an extremely low permeation ratio (< 5%) of both cell types was found with the use of surface-modified or unmodified PU foaming membranes with a 12-μm pore size. It was also found that the nylon-net filter had screen-like pore structure, whereas the PU membranes had a deformed open pore structure. This indicates that not only the pore size but also the pore morphology is important for membrane-based cell separation.

Even a small degree of enrichment, such as the separation factor of 1.8, is also considered effective in the transplantation of mesenchymal cells in clinical application, although clinical trials using the enriched-cell type of mesenchymal cells have not yet been performed. In conclusion, cell separation between mesenchymal progenitor cells through porous polymeric membranes was shown to be possible in this study. This technology will contribute to the future clinical application of cell transplantation into the damaged tissue of patients.

REFERENCES

1. Umezawa A, Maruyama T, Segawa K, Shadduck RK, Waheed A, Hata J. Multipotent marrow stromal cell is able to induce hematopoiesis *in vivo*. J Cell Physiol 1992;151:197–205.
2. Kohyama J, Abe H, Shimazaki T, Koizumi A, Nakashima K, Gojo S, Taga T, Okano H, Hata J, Umezawa A. Brain from bone: Efficient "meta-differentiation" of marrow stroma-derived mature osteoblasts to neurons with Noggin or a demethylating agent. Differentiation 2001;68:235–244.
3. Edwards M, Twin J, Wilkinson S. New technique to assess the axilla for breast cancer metastases using cell separation technology. Aust N Z J Surg 2002;72:655–659.
4. Vij R, Brown R, Shenoy S, Haug JS, Kaesberg D, Adkins D, Goodnough LT, Khoury H, DiPersio J. Allogeneic peripheral blood stem cell transplantation following CD34$^+$ enrichment by density gradient separation. Bone Marrow Transplant 2000; 25:1223–1228.
5. Sanada Y. Transplantation of hematopoietic cells: General theory. In: Harada M, Katoh S, Sanada Y, editors. New trends in hematopoietic stem cell transplantation. Tokyo: Nanoudo: 1998. p 1–7.
6. Gryn J, Shadduck RK, Lister J, Zeigler ZR, Raymond JM. Factors affecting purification of CD34$^+$ peripheral blood stem cells using the Baxter Isolex 300i. J Hematother Stem Cell Res 2002;11:719–730.
7. Carreras E, Saiz A, Marin P, Martinez C, Rovira M, Villamor N, Aymerich M, Lozano M, Fernandez-Aviles F, Urbano-Izpizua A, Montserrat E, Graus F. CD34$^+$ selected autologous

peripheral blood stem cell transplantation for multiple sclerosis: report of toxicity and treatment results at one year of follow-up in 15 patients. Haematologica 2003;88:306–314.
8. Domingo JC, Mercadal M, Petriz J, De Madariaga MA. Preparation of PEG-grafted immunomagnetoliposomes entrapping citrate stabilized magnetite particles and their application in $CD34^+$ cell sorting. J Microencapsul 2001;18:41–54.
9. Comella K, Nakamura M, Melnik K, Chosy J, Zborowski M, Cooper MA, Fehniger TA, Caligiuri MA, Chalmers JJ. Effects of antibody concentration on the separation of human natural killer cells in a commercial immunomagnetic separation system. Cytometry 2001;45:285–293.
10. Kataoka K, Sakurai Y, Hanai T, Maruyama A, Tsuruta T. Immunoaffinity chromatography of lymphocyte subpopulations using *tert*-amine derived matrices with adsorbed antibodies. Biomaterials 1988;9:218–224.
11. Ohba H, Bakalova R, Moriwaki S, Nakamura O. Fractionation of normal and leukemic T-cells by lectin-affinity column chromatography. Cancer Lett 2002;184:207–214.
12. Komai H, Naito Y, Fujiwara K, Takagaki Y, Noguchi Y, Nishimura Y. The protective effect of a leucocyte removal filter on the lung in open-heart surgery for ventricular septal defect. Perfusion 1998;13:27–34.
13. Muller-Steinhardt M, Hennig H, Kirchner H, Schlenke P. Prestorage WBC filtration of RBC units with soft-shell filters: filtration performance and impact on RBCs during storage for 42 days. Transfusion 2002;42:153–158.
14. Higuchi A, Yamamiya S, Yoon BO, Sakurai N, Hara M. Peripheral blood cell separation through surface-modified polyurethane membranes. J Biomed Mater Res 2004;68:34–42.
15. Kiyohara S, Sasaki M, Saito K, Sugita K, Sugo T. Radiation-induced grafting of phenylalanine-containing monomer onto a porous membrane. Reactive Functional Polym 1996;31:103–110.
16. Kim M, Kiyohara S, Konishi S, Tsuneda S, Saito K, Sugo T. Ring-opening reaction of poly-GMA chain grafted onto a porous membrane. J Membrane Sci 1996;117:33–38.
17. Higuchi A, Takanashi Y, Tsuzuki N, Asakura T, Cho CS, Akaike T, Hara M. Production of interferon-β by fibroblast cells on membranes prepared with RGD-containing peptides. J Biomed Mater Res 2003;65:369–378.
18. Higuchi A, Takanashi Y, Ohno T, Asakura T, Cho CS, Akaike T, Hara M. Production of interferon-β by fibroblast cells on the membranes prepared by extracellular matrix proteins. Cytotechnology 2002;39:131–137.
19. Higuchi A, Tamiya S, Tsubomura T, Katoh A, Cho CS, Akaike T, Hara M. Growth of L929 cells on polymeric films prepared by Langmuir-Blodgett and casting methods. J Biomater Sci Polym Ed 2000;11:149–168.
20. Higuchi A, Shirano K, Harashima M, Yoon BO, Hara M, Hattori M, Imamura K. Chemically modified polysulfone hollow fibers with vinylpyrrolidone having improved blood compatibility. Biomaterials 2002;23:2659–2666.
21. Keeney M, Chin-Yee I, Weir K, Popma J, Nayar R, Sutherlamd DR. Single platform flow cytometric absolute $CD34^+$ cell counts based on the ISAHE guidelines. Cytometry 1998; 34:61–70.

Available online at www.sciencedirect.com
SCIENCE DIRECT®
ELSEVIER
Cancer Letters 221 (2005) 21–28
CANCER Letters
www.elsevier.com/locate/canlet

Effects of 3-methylcholanthrene on the transcriptional activity and mRNA accumulation of the oncogene *hWAPL*

Masahiko Kuroda[a,b,c,*], Kosuke Oikawa[a,b,c], Keiichi Yoshida[a,c], Aya Takeuchi[d], Masaru Takeuchi[d], Masahiko Usui[d], Akihiro Umezawa[c,e], Kiyoshi Mukai[a]

[a]*Department of Pathology, Tokyo Medical University, 6-1-1 Shinjuku, Shinjuku-ku, Tokyo 160-8402, Japan*
[b]*CREST Research Project, Japan Science and Technology Corporation, 4-1-6 Kawaguchi, Saitama 332-0012, Japan*
[c]*Shinanomachi Research Park, Keio University, 35 Shinanomachi, Shinjuku-ku, Tokyo 160-8582, Japan*
[d]*Department of Ophthalmology, Tokyo Medical University, 6-7-1 Nishi-shinjuku, Shinjuku-ku, Tokyo 160-0023, Japan*
[e]*National Research Institute for Child Health and Development, 3-35-31 Taishido, Setagaya-ku, Tokyo 154-8567, Japan*

Received 28 April 2004; received in revised form 26 July 2004; accepted 5 August 2004

Abstract

hWAPL is a human oncogene associated with uterine cervical cancer. Here, we demonstrate that *hWAPL* transcription is induced by 3-methylcholanthrene (3-MC) in the cervical carcinoma-derived cell line SiHa. *hWAPL* transcription was analyzed with evaluation of the mRNA and heterogeneous nuclear RNA (hnRNA) levels by quantitative real time PCR analysis. Flow cytometric analysis suggested that the alteration of *hWAPL* mRNA levels is independent of cell cycle profile. We also found that DMSO and some components of FBS affect *hWAPL* transcription. Interestingly, when the aryl hydrocarbon receptor (AhR) function was inhibited by α-naphthoflavone (ANF), the induction of *hWAPL* transcription by 3-MC was greater than that in AhR-functioning normal cells. These observations suggest that there are complex mechanisms regulating the transcription of *hWAPL*. Furthermore, mRNA level of a mouse homolog of *hWAPL* in mouse uterus was induced by 3-MC injection into the abdominal cavity. Thus, some effects from 3-MC exposure on uterus may be mediated by the unscheduled overexpression of *hWAPL*.

Keywords: 3-Methylcholanthrene (3-MC); hWAPL; Uterine cervical cancer; Aryl hydrocarbon receptor (AhR); α-naphthoflavone (ANF)

1. Introduction

Previously, we have isolated and characterized a novel human gene termed *hWAPL* [1]. Our initial observations suggested that *hWAPL* expression is associated with uterine cervical cancer, although the mechanism was not clear. *hWAPL* is the human homolog of the *wings apart-like* (*wapl*) gene in

* Corresponding author. Address: Department of Pathology, Tokyo Medical University, 6-1-1 Shinjuku, Shinjuku-ku, Tokyo 160-8402, Japan. Tel.: +81 3 3351 6141x425; fax: +81 3 3352 6335.
E-mail address: kuroda@tokyo-med.ac.jp (M. Kuroda).

0304-3835/$ - see front matter © 2004 Elsevier Ireland Ltd. All rights reserved.
doi:10.1016/j.canlet.2004.08.006

Drosophila melanogaster. The protein encoded by *wapl* controls heterochromatin organization and was identified as a modifier of both PEV and chromosome inheritance [2,3]. Thus, hWAPL is also expected to be involved in heterochromatin maintenance and epigenetic control.

Polycyclic aromatic hydrocarbons (PAHs) are carcinogenic and immunotoxic chemicals widely distributed in the environment [4]. 3-Methylcholanthrene (3-MC) is one of the most toxic and the best-studied compounds in the PAHs. Most of the toxic effects of PAHs are mediated by the aryl hydrocarbon receptor (AhR) [5]. When PAHs bind to the AhR, the ligated AhR translocates from the cytoplasm to the nucleus where it switches its partner molecule from heat shock protein 90 kD (Hsp90) to the aryl hydrocarbon receptor nuclear translocator (Arnt) [6]. The resulting AhR/Arnt heterodimer binds a specific DNA sequence, designated xenobiotic responsive element (XRE), in the promoter region of target genes to enhance their expression [6]. On the other hand, several studies have suggested the existence of AhR independent pathways for PAH toxicity [7,8]. In all cases, many of the putative target genes responsible for the toxicity symptoms have yet to be identified.

In the present study, we demonstrate that *hWAPL* is a target gene of 3-methylcholanthrene. The results suggest that carcinogenesis by 3-MC may involve alterations of *hWAPL* gene expression.

2. Materials and methods

2.1. Chemicals

3-Methylcholanthrene (Sigma-Aldrich Japan, Tokyo, Japan) was prepared in dimethylsulfoxide (DMSO) for cultured cells and in olive oil for treatment of mice. Aphidicolin (Wako Pure Chemical Industries, Ltd, Osaka, Japan), Nocodazole (Sigma Chemical Co., St Louis, MO) and α-naphthoflavone (Sigma) were prepared in DMSO.

2.2. Cell cultures

The human uterine cervical carcinoma-derived cell lines, SiHa, CaSki and HeLa cells, were obtained from American Type Culture Collection (ATCC), and grown in DMEM (Sigma) supplemented with 10% fetal bovine serum (FBS) (Trace Scientific Ltd, Melbourne, Australia) at 37 °C in a 5% CO_2 environment. Where indicated, SiHa cells were grown in DMEM supplemented with 10% charcoal/dextran treated FBS (CTF) (Biosource, Rockville, MD) or 0.4% (w/v) bovine serum albumin (BSA) (Trace) instead of FBS.

2.3. Immunoblot analysis

Protein samples were prepared as previously described [9]. Immunoblot analysis was performed as previously described [1].

2.4. Flow cytometric analysis

To determine cell cycle profiles, cells at different time points were harvested, washed, and fixed with a solution containing 70% ethanol and 30% PBS. After incubation overnight at 4 °C, cells were suspended in staining buffer (propidium iodide, 50 μg/ml; RNaseA, 0.1%; glucose, 1 mg/ml in PBS). Then, after incubation for 30 min at room temperature, the cells were analyzed with a FACS Vantage flow cytometer using the Cell Quest acquisition and analysis program (BD Biosciences, San Jose, CA).

2.5. Animals and treatment

C57/BL6 female mice (6 weeks old) were purchased from Oriental Yeast Co., Ltd (Tokyo, Japan). The mice received a single intraperitoneal injection of 1 ml of olive oil containing 3-MC at a dose of 80 mg/kg of body mass. The control mice were injected with olive oil alone. Uterus samples were harvested 24 and 48 h after injection and subjected to real time PCR analysis.

2.6. RNA isolation and quantitative real time PCR

First strand cDNA synthesis was performed as described [10] using M-MLV Reverse transcriptase (Invitrogen Japan, Tokyo, Japan) with Oligo $(dT)_{17}$ (for Figs. 1–3 and 6) or Random Primers (Invitrogen) (for Figs. 4 and 5).

Real time PCR analysis for *hWAPL* and human β-*actin* mRNAs was performed as described [1]

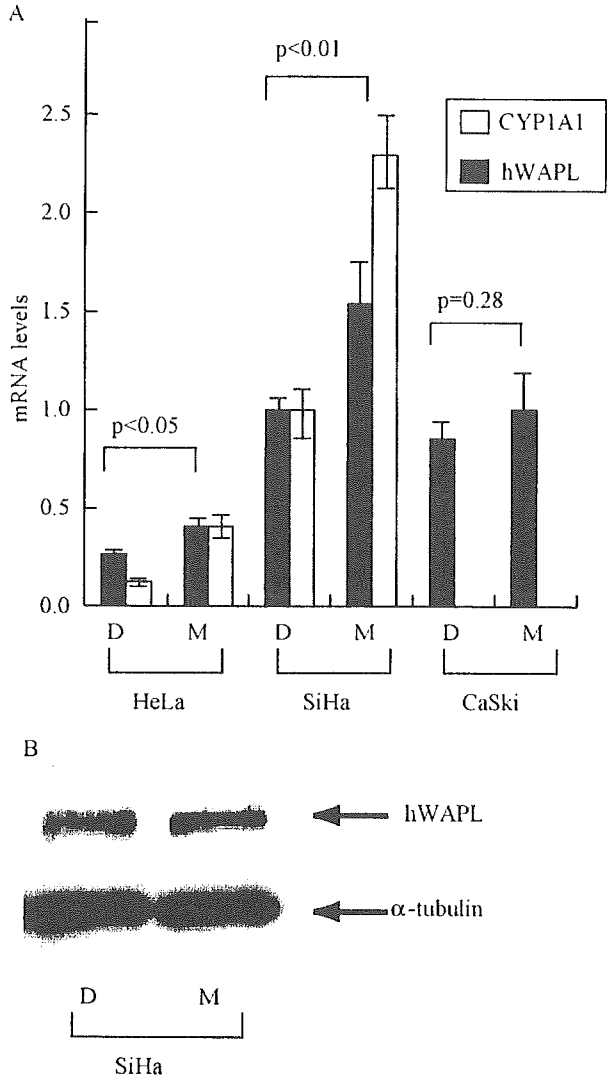

Fig. 1. Effects of 3-MC on *hWAPL* expression in the human cervical cancer-derived cell lines. D, DMSO alone; M, 3-MC. (A) HeLa, SiHa and CaSki cells were treated with 0.1% DMSO alone or 1 μM of 3-MC for 6 h. Then, the *hWAPL* and *CYP1A1* mRNA levels in the cells were evaluated by quantitative real time PCR analysis. Data were normalized to the mRNA levels of SiHa cells treated with DMSO alone that was arbitrarily set to 1 in the graphical presentation. *Bars, s.e.* (B) SiHa cells were treated with 0.1% DMSO alone or 1 μM 3MC for 6 h, and then the protein samples were prepared and subjected to western blotting analysis. α-tubulin was also shown as a loading control.

except for the 40 PCR cycles at 95 °C for 3 s and 68 °C for 30 s. Real Time PCR analysis for human *CYP1A1* mRNA and *hWAPL* hnRNA was also performed with the same PCR protocol. The nucleotide sequences of primers specific for human *CYP1A1* mRNA were previously described [11]. Primers specific for *hWAPL* hnRNA are 5′-GAGATTACACCACTGCACTCC-3′ and 5′-TTGCTCCCACTTACTATGGCC-3′. For mouse cDNAs, we used primers specific for the mouse homolog of *hWAPL* mRNA, 5′-ACCTGGTGGAGTATAGTGCCC-3′ and 5′-TGGCAGAGACACCCAAGAAGC-3′ (The nucleotide sequences were obtained from mKIAA0261 in Database), mouse β-*actin* mRNA, 5′-AGCCTTCCTTCTTGGGTATGG-3′ and 5′-CACTTGCGGTGCACGATGGAG-3′, and mouse *CYP1A1* mRNA, 5′-TTTGGTTTGGGCAAGCGA-3′ and 5′-GTCTAAGCCTGAAGATGC-3′. Reaction mixtures were denatured at 95 °C for 30 s then subjected to 40 PCR cycles at 95 °C for 3 s, 68 °C for 30 s, and 86 °C for 6 s for mouse *WAPL* mRNA, and at 95 °C for 3 s, 68 °C for 30 s, and 85 °C for 6 s for mouse β-*actin* and *CYP1A1* mRNAs, respectively. *hWAPL, mouse WAPL* and human and mouse *CYP1A1* mRNA levels and *hWAPL* hnRNA level were normalized to human and mouse β-*actin* signals, respectively. The absence of PCR products after the PCR on non-reverse-transcribed total RNA served as a routine check for contaminating genomic DNA. We performed the experiments to determine mRNA and hnRNA levels in triplicate.

The data were analyzed using Student's-*t* test, and $Ps < 0.05$ were considered to indicate significant differences.

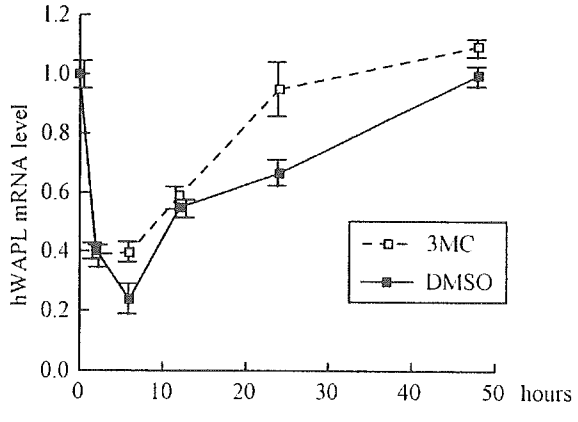

Fig. 2. Kinetics of *hWAPL* mRNA levels in SiHa cells at several time points after treatment with DMSO alone or 1 μM of 3-MC. The *hWAPL* mRNA levels in the cells were evaluated by quantitative real time PCR analysis. Data were normalized to the mRNA level at 0 h that was arbitrarily set to 1 in the graphical presentation. *Bars, s.e.*

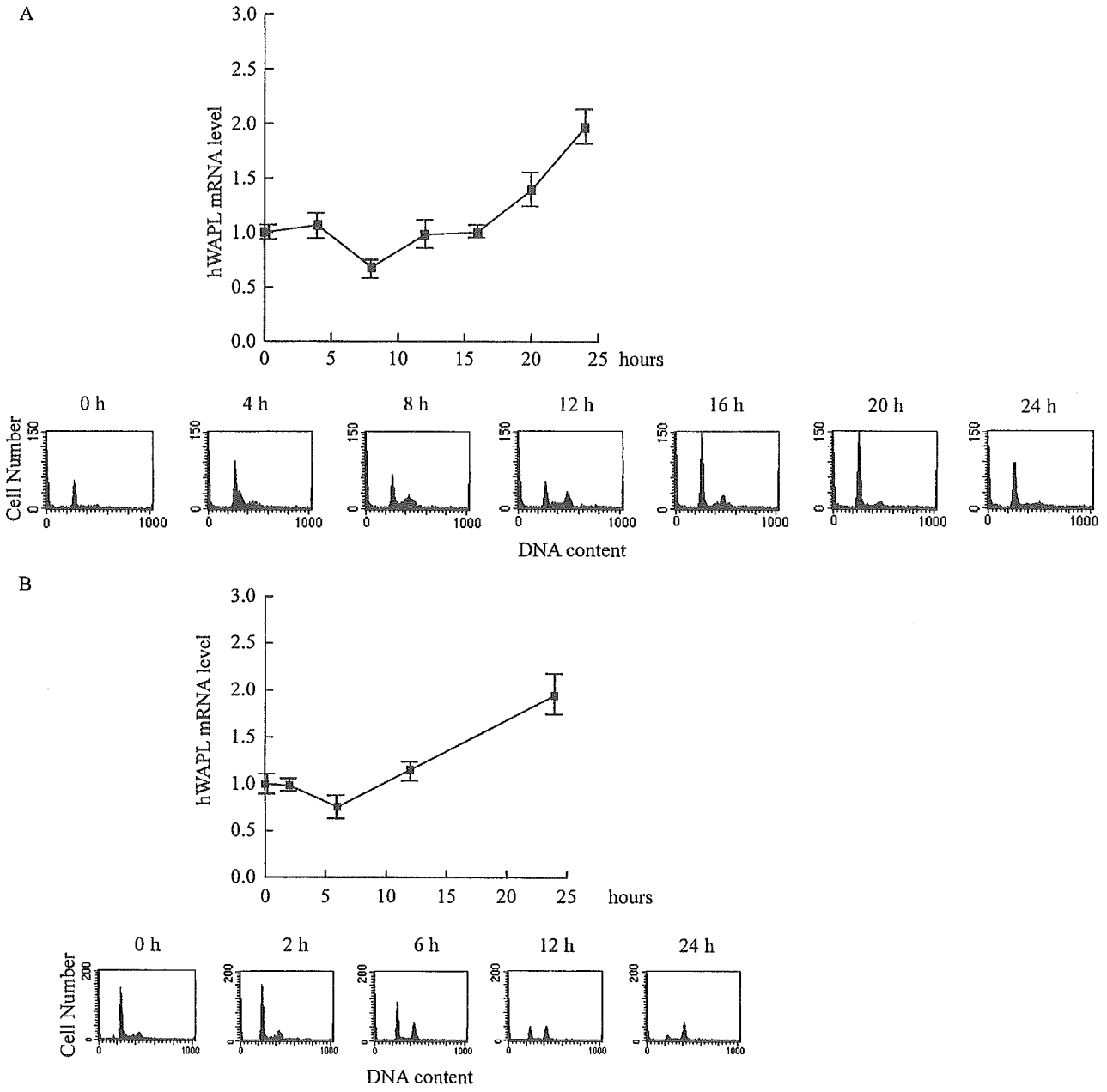

Fig. 3. Cell cycle profiles and *hWAPL* mRNA levels. *hWAPL* mRNA levels in the cells were determined by real time PCR analysis. Data were normalized to the mRNA level at 0 h that was arbitrarily set to 1 in the graphical presentation. *Bars, s.e.*. Cell cycle profiles of the cells at each time points were also confirmed by flow cytometric analysis. (A) Kinetics of *hWAPL* mRNA levels in SiHa cells at 0, 4, 8, 12, 16, 20 and 24 h after releasing from G1 arrest by 1 μg/ml aphidicolin treatment. (B) Kinetics of *hWAPL* mRNA levels in SiHa cells at 0, 2, 6, 12 and 24 h after 50 ng/ml nocodazole treatment.

3. Results and discussion

To examine whether 3-MC affects *hWAPL* expression, we treated various human uterine cervical cancer-derived cell lines with dimethylsulfoxide (DMSO) alone or 3-MC for 6 h. Then, we calculated the amounts of the *hWAPL* mRNAs in the cells by quantitative real time PCR analysis, and found that *hWAPL* mRNA levels were increased in the 3-MC-treated cells (Fig. 1A). The increases in *hWAPL* mRNA levels in SiHa cells was most remarkable among the cell lines examined. Because the *CYP1A1* gene is

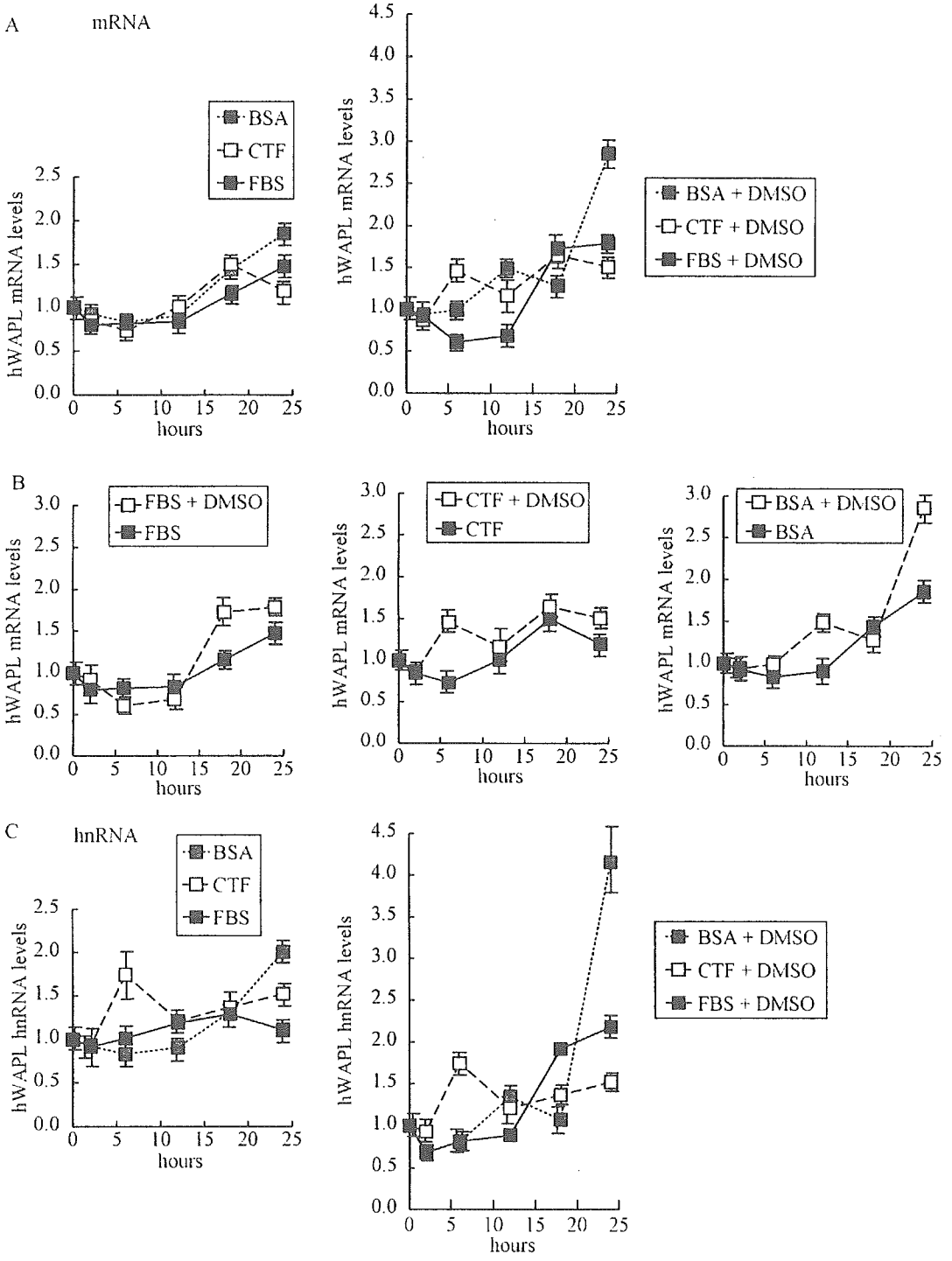

Fig. 4. Effects of FBS, CTF, BSA and DMSO on *hWAPL* mRNA and hnRNA levels in SiHa cells. *hWAPL* mRNA and hnRNA levels in SiHa cells at 0, 2, 6, 12, 18 and 24 h after replacing the growth medium to a fresh medium supplemented with FBS, CTF or BSA with or without 0.1% DMSO were deteremined by real time PCR analysis. Data were normalized to the mRNA and hnRNA level at 0 h that was arbitrarily set to 1 in the graphical presentation. *Bars, s.e.* (A) Kinetics of the *hWAPL* mRNA levels in the cells grown in the growth medium supplemented as indicated. (B) Graphical representation of the effects of DMSO on the kinetics of *hWAPL* mRNA levels in the cells grown in the growth medium supplemented with FBS, CTF or BSA. (C) Kinetics of the *hWAPL* hnRNA levels in the cells grown in the growth medium supplemented as indicated.

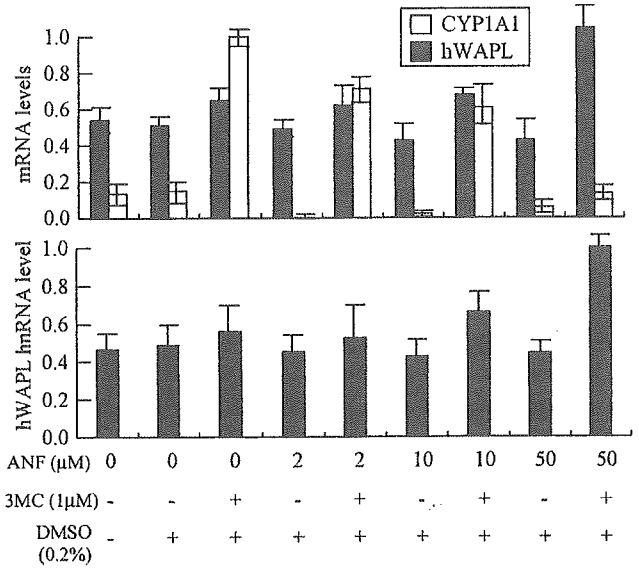

Fig. 5. Effects of AhR inhibition by α-naphthoflavone on *hWAPL* mRNA and hnRNA levels in SiHa cells treated with 3-MC. SiHa cells were treated with 0.2% DMSO alone or 1 μM 3-MC with 0. 2, 10 or 50 μM ANF for 6 h. Then, the *hWAPL* mRNA and hnRNA levels and the *CYP1A1* mRNA levels were deteremined by real time PCR analysis. SiHa cells grown for 6 h in a normal fresh medium without chemicals were also analyzed as a normal control. Data were normalized to the maximaum mRNA and hnRNA levels that were arbitrarily set to 1 in the graphical presentation. *Bars, s.e.*

a well-known target of 3-MC [12,13], we also calculated *CYP1A1* mRNA levels in the three cell lines to confirm the effects of 3-MC on the cells (Fig. 1A). We found that *CYP1A1* mRNA levels in SiHa cells were highest and increased most remarkable. *CYP1A1* mRNA in CaSki cells was not detected in our experiments. We also observed that hWAPL protein level was increased in the 3-MC-treated SiHa cells (Fig. 1B).

We next examined the effects of 3-MC on *hWAPL* expression in SiHa cells at several time points after 3-MC treatment (Fig. 2). The 3-MC-treated cells showed higher levels of *hWAPL* mRNA than the control cells at all time points examined. Interestingly, the *hWAPL* mRNA levels decreased first 6 h and then increased after changing the medium to a fresh medium containing DMSO with or without 3-MC as seen in Fig. 2.

These results prompted us to investigate whether the *hWAPL* expression is related to the cell cycle. First, to synchronize cell cycle progression, we treated SiHa cells with aphidicolin, an inhibitor of DNA synthesis, for 12 h to induce G1-phase arrest. We then released the cells from G1 arrest by changing the culture medium to a fresh growth medium. The synchronized cells were harvested every 4 h for 24 h after release from aphidicolin, and the *hWAPL* mRNA levels were calculated by quantitative real time PCR analysis (Fig. 3A). As seen in Fig. 3A, *hWAPL* mRNA initially decreased and then increased over time. Flow cytometric analysis confirmed the cell cycle phase of the cells at each time point (Fig. 3A). From these results, *hWAPL* mRNA level seemed to fluctuate in accordance with cell cycle profile. However, the levels of *hWAPL* mRNA in the cells treated with nocodazole, an inhibitor of spindle assembly, fluctuated in a similar manner to the aphidicolin-synchronized cells (Fig. 3B). Thus, amounts of *hWAPL* mRNAs are likely to have no relation to the cell cycle profiles. Recently, Guigal et al. demonstrated that FBS induces transcription of the *CYP1A1* gene. Therefore, we suspected that the fluctuation of *hWAPL* mRNA levels might be associated with the culture medium change.

To investigate the effects of components in FBS on the fluctuation of *hWAPL* mRNA levels, we examined the *hWAPL* mRNA levels in SiHa cells after changing growth medium to a fresh medium supplemented with charcoal/dextran treated FBS (CTF) or BSA instead of FBS. The fluctuations of the *hWAPL* mRNA levels showed similar trends among the cells grown with FBS, CTF and BSA (Fig. 4A; left panel). However, all cells examined in Figs. 1–3 were grown in the medium containing DMSO. Thus, we also tested the effects of DMSO with FBS, CTF or BSA at the same time. Interestingly, fluctuations of the *hWAPL* mRNA levels in SiHa cells treated with 0.1% DMSO showed different trends among FBS, CTF and BSA (Fig. 4A; right panel), and the *hWAPL* mRNA levels in the DMSO-treated cells fluctuated more drastically than that in the cells grown without DMSO (Fig. 4B). Especially, remarkable decrease of *hWAPL* mRNA levels for first 6 h after the medium change was distinctive for the growth medium supplemented with FBS and DMSO. These results suggest that DMSO and some constituents of FBS affect *hWAPL* mRNA accumulation synergistically.

mRNA levels do not always reflect on the transcription activity of genes. To investigate the kinetics of the promoter activities of the *hWAPL* gene in the cells, we evaluated the levels of *hWAPL* heterogeneous nuclear RNA (hnRNA), the unprocessed precursor of the mature and functional mRNA,

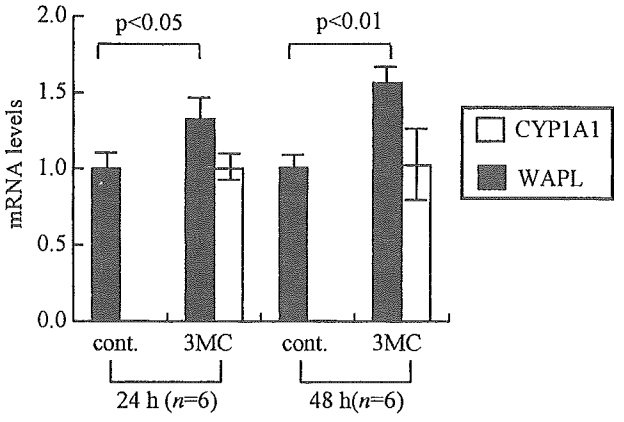

Fig. 6. Effects of 3-MC on *WAPL* mRNA levels in mouse uteri. The mice received a single intraperitoneal injection of 1 ml of olive oil containing 3-MC (3-MC) or olive oil only (cont.), and *WAPL* mRNA levels in the uteri at 24 and 48 h after injection were determined with quantitative real time PCR analysis. *CYP1A1* mRNA levels were also deteremined to confirm the effects of 3-MC on mouse uteri. The data represent the means of multiple samples normalized to the mean values of the *hWAPL* mRNA levels in the cont. 24 h samples and *CYP1A1* mRNA levels in the 3-MC 24 h samples, respectively, that were arbitrarily set to 1 in the graphical presentation. *Bars, s.e.*

by real time PCR using intron-specific primers for *hWAPL* searched in Ensembl Genome Browser (http://www.ensembl.org/). Levels of hnRNA have been proposed as a surrogate for nuclear run-on assays to determine gene transcription rates [14,15]. Although the *hWAPL* hnRNA levels fluctuated in somewhat different manner to the mRNA levels in the cells grown without DMSO, the *hWAPL* hnRNA levels in the DMSO-treated cells fluctuated in similar manner to the mRNA levels (Fig. 4C; compare with Fig. 4A). These results suggest that DMSO and some components of FBS affect transcriptional activity of the *hWAPL* gene. Increase of *hWAPL* transcription levels at 24 h in common with the cells under various conditions may be caused by the accumulation of wastes in their growth medium.

3-MC is known to be an agonist of AhR [16]. Thus, to investigate whether AhR is related to *hWAPL* transcription activation, we examined the effects of α-naphthoflavone (ANF), an AhR antagonist [17], at a dose of 2, 10 and 50 μM on *hWAPL* mRNA and hnRNA levels in 3-MC-treated SiHa cells by quantitative real time PCR analysis (Fig. 5). We also evaluated *CYP1A1* mRNA levels for monitoring the inhibitory effects on AhR functions by ANF, and found that 50 μM of ANF strongly inhibited AhR functions (Fig. 5; upper panel). Interestingly, increase of *hWAPL* mRNA levels by 3-MC was more remarkable in AhR-inhibited cells rather than that in AhR-functioning normal cells. Induction of *hWAPL* hnRNA levels showed similar manner to the *hWAPL* mRNA (Fig. 5; lower panel). From these results, we hypothesized that AhR was involved in the transcriptional regulation of *hWAPL*, but there are complex mechanisms for the transcriptional regulation of *hWAPL*. We did not find XRE motif in 5000 bp of 5′-upstream sequence of the *hWAPL* gene using MOTIF Sequence Motif Search (http://motif.genome.jp/) at the cut off score 85. Thus, although further investigation is required, we suppose that *hWAPL* is not a direct target of 3-MC but a down stream molecule of a 3-MC-targeted molecule.

Finally, we examined whether the mRNA level of a mouse homolog of *hWAPL* is increased by 3-MC in mouse uterus. Twenty-four and 48 h after the injection of 3-MC into the abdominal cavities of C57/BL6 female mice, we harvested the uteri and analyzed the *WAPL* mRNA levels by quantitative real time PCR analysis. The *CYP1A1* mRNA levels were also analyzed to confirm the 3-MC effects on the uteri. The uteri exhibited increases in *WAPL* mRNA levels compared with that of control mice (Fig. 6). These data suggest that 3-MC exposure affects *WAPL* expression in uterus.

Our recent data demonstrated that the unscheduled increase of *hWAPL* expression in human uterine cervix is associated with cervical cancer [1]. In Addition, previous studies demonstrated that 3-MC induces carcinogenesis in mouse uterine cervix [18, 19]. Thus, although the *hWAPL* induction by 3-MC was weak in our experiments, our results suggest that the promotion of carcinogenesis by 3-MC in uterus is likely to involve the *hWAPL* oncogene.

Acknowledgements

This work was supported by a Grant-in-Aid for scientific research on Priority Area (C) from the Ministry of Education, Science, Sports and Culture, and a grant from Core Research for Evolutional Science and Technology (CREST), Japan Science and Technology Corporation.

References

[1] K. Oikawa, T. Ohbayashi, T. Kiyono, H. Nishi, K. Isaka, A. Umezawa, et al., Expression of a novel human gene, human wings apart-like (hWAPL), is associated with cervical carcinogenesis and tumor progression, Cancer Res. 64 (2004) 3545–3549.

[2] F. Verni, R. Gandhi, M.L. Goldberg, M. Gatti, Genetic and molecular analysis of wings apart-like (wapl), a gene controlling heterochromatin organization in *Drosophila melanogaster*, Genetics 154 (2000) 1693–1710.

[3] K.W. Dobie, C.D. Kennedy, V.M. Velasco, T.L. McGrath, J. Weko, R.W. Patterson, G.H. Karpen, Identification of chromosome inheritance modifiers in *Drosophila melanogaster*, Genetics 157 (2001) 1623–1637.

[4] S. Reynaud, C. Duchiron, P. Deschaux, 3-Methylcholanthrene increases phorbol 12-myristate 13-acetate-induced respiratory burst activity and intracellular calcium levels in common carp (Cyprinus carpio L) macrophages, Toxicol. Appl. Pharmacol. 175 (2001) 1–9.

[5] J. Mimura, Y. Fujii-Kuriyama, Functional role of AhR in the expression of toxic effects by TCDD, Biochim. Biophys. Acta 1619 (2003) 263–268.

[6] K. Sogawa, Y. Fujii-Kuriyama, Ah receptor, a novel ligand-activated transcription factor, J. Biochem. (Tokyo) 122 (1997) 1075–1079.

[7] K. Oikawa, T. Ohbayashi, J. Mimura, R. Iwata, A. Kameta, K. Evine, et al., Dioxin suppresses the checkpoint protein, MAD2, by an aryl hydrocarbon receptor-independent pathway, Cancer Res. 61 (2001) 5707–5709.

[8] S.R. Kondraganti, P. Fernandez-Saluguero, F.J. Gonzalez, K.S. Ramos, W. Jiang, B. Moorthy, Polycyclic aromatic hydrocarbon-inducible DNA adducts: evidence by 32P-postlabeling and use of knockout mice for Ah receptor-independent mechanisms of metabolic activation in vivo, Int. J. Cancer 103 (2003) 5–11.

[9] K. Oikawa, T. Ohbayashi, J. Mimura, Y. Fujii-Kuriyama, S. Teshima, K. Rokutan, et al., Dioxin stimulates synthesis and secretion of IgE-dependent histamine-releasing factor, Biochem. Biophys. Res. Commun. 290 (2002) 984–987.

[10] M. Kuroda, T. Ishida, M. Takanashi, M. Satoh, R. Machinami, T. Watanabe, Oncogenic transformation and inhibition of adipocytic conversion of preadipocytes by TLS/FUS-CHOP type II chimeric protein, Am. J. Pathol. 151 (1997) 735–744.

[11] K. Oikawa, Y. Kosugi, T. Ohbayashi, A. Kameta, K. Isaka, M. Takayama, et al., Increased expression of IgE-dependent histamine-releasing factor in endometriotic implants, J. Pathol. 199 (2003) 318–323.

[12] N. Guigal, E. Seree, V. Bourgarel-Rey, Y. Barra, Induction of CYP1A1 by serum independent of AhR pathway, Biochem. Biophys. Res. Commun. 267 (2000) 572–576.

[13] N. Guigal, E. Seree, Q.B. Nguyen, B. Charvet, A. Desobry, Y. Barra, Serum induces a transcriptional activation of CYP1A1 gene in HepG2 independently of the AhR pathway, Life Sci. 68 (2001) 2141–2150.

[14] C.J. Elferink, J.J. Reiners Jr., Quantitative RT-PCR on CYP1A1 heterogeneous nuclear RNA: a surrogate for the in vitro transcription run-on assay, Biotechniques 20 (1996) 470–477.

[15] R.F. Johnson, C.M. Mitchell, W.B. Giles, W.A. Walters, T. Zakar, The in vivo control of prostaglandin H synthase-2 messenger ribonucleic acid expression in the human amnion at parturition, J. Clin. Endocrinol. Metab. 87 (2002) 2816–2823.

[16] M. Naruse, Y. Ishihara, S. Miyagawa-Tomita, A. Koyama, H. Hagiwara, 3-Methylcholanthrene, which binds to the arylhydrocarbon receptor, inhibits proliferation and differentiation of osteoblasts in vitro and ossification in vivo, Endocrinology 143 (2002) 3575–3581.

[17] T.A. Gasiewicz, G. Rucci, Alpha-naphthoflavone acts as an antagonist of 2,3,7, 8-tetrachlorodibenzo-p-dioxin by forming an inactive complex with the Ah receptor, Mol. Pharmacol. 40 (1991) 607–612.

[18] P. Das, A.R. Rao, P.N. Srivastava, Influence of ascorbic acid on MCA-induced carcinogenesis in the uterine cervix of mice, Cancer Lett. 72 (1993) 121–125.

[19] S. Gagandeep, S. Dhanalakshmi, E. Mendiz, A.R. Rao, R.K. Kale, Chemopreventive effects of Cuminum cyminum in chemically induced forestomach and uterine cervix tumors in murine model systems, Nutr. Cancer 47 (2003) 171–180.

J Bone Miner Metab (2005) 23:123–133
DOI 10.1007/s00774-004-0550-y

ORIGINAL ARTICLE

**Nobuyuki Kawashima · Kentaro Shindo · Kei Sakamoto
Hisatomo Kondo · Akihiro Umezawa · Shohei Kasugai
Bernard Perbal · Hideaki Suda · Minoru Takagi
Ken-ichi Katsube**

Molecular and cell biological properties of mouse osteogenic mesenchymal progenitor cells, Kusa

Received: March 15, 2004 / Accepted: September 9, 2004

Abstract A cell line of murine osteogenic progenitor cells, Kusa, was established from femoral bone marrow stromal cells with other types of mesenchymal progenitor cells. We characterized two sublines of Kusa (Kusa-A1 and Kusa-O) from several aspects, including the use of an expression profiling system, a cDNA microarray. The original Kusa subline (Kusa-A1) had high alkaline phosphatase activity and high accumulation of calcium deposits in a condition inducing mineralization, with ascorbic acid and β-glycerophosphate. Kusa-O, a low osteogenic subline of Kusa, had high alkaline phosphatase activity but slow accumulation of calcium deposits even in the inducing condition. These two Kusa sublines differed in the expression of the osteogenic marker genes, *osteocalcin* and *osteopontin*, during mineralization. A type of cDNA microarray revealed marked downregulation of gene expression in the inducing condition in both Kusa-A1 and Kusa-O. Another type of high-throughput microarray was performed to examine the difference in gene expression patterns between Kusa-A1 and Kusa-O. By this analysis, *periostin*, which would be involved in a stage of osteogenesis, was low in Kusa-A1. On the contrary, *Myocyte enhancer factor 2C (MEF2C)*, a myogenic transcriptional factor, was high in Kusa-A1, although no expression of any other myogenic genes was shown.

Key words Osteogenesis · Stem cells · Notch · MEF2 · Periostin

N. Kawashima (✉) · K. Shindo · H. Suda
Pulp Biology and Endodontics, Graduate School of Tokyo Medical and Dental University, 1-5-45 Yushima, Bunkyo-ku, Tokyo 113-8549, Japan
Tel./Fax +81-3-5803-5494
e-mail: kawashima.n.endo@tmd.ac.jp

N. Kawashima
Center of Excellence Program for Research on Molecular Destruction and Reconstruction of Tooth and Bone, Graduate School of Tokyo Medical and Dental University, Tokyo, Japan

A. Umezawa
Department of Reproductive Biology and Pathology, National Institute for Child Health and Development, Tokyo, Japan

B. Perbal
Laboratorie d'Oncologie Virale et Moléculaire, UFR de Biochimie, Université Paris, Paris, France

K. Sakamoto · M. Takagi · K. Katsube
Molecular Pathology, Graduate School of Tokyo Medical and Dental University, Tokyo, Japan

H. Kondo · S. Kasugai
Masticatory Function Control, Graduate School of Tokyo Medical and Dental University, Tokyo, Japan

N. Kawashima and K. Katsube contributed equally to this work

Introduction

The ability of mesenchymal progenitor cells to differentiate has been the subject of a growing body of documents that have revealed the unexpected potential of bone marrow cells [1,2]. Bone marrow stromal cells support the growth and differentiation of hematopoietic stem cells by both direct and indirect influences [3], and they themselves can differentiate into various types of cells, i.e., striated muscle [4], heart muscle [5], bone tissue [6], chondroctytes [7], and even neurons [8] or hepatocytes [9]. However, few studies have been done about the molecular basis of their potential, and this potential is a puzzle, considering their paradoxical stability (cells that have pluripotency but keep the quiescent state in situ) [7,10]. Further more, bone marrow progenitor cells were demonstrated to be involved in the recovery of blood vessel injury, although they caused atherosclerosis [11]. Thus, it seems that mesenchymal progenitor cells sometimes generate pathogenic change, and it is necessary to investigate their activity from a non-restitutive aspect.

The factors that regulate the potential of mesenchymal progenitor cells have been investigated in various ways. Among them, myogenesis was well-examined at a molecular level, using C3H10T1/2, a murine pluripotent fibroblastic cell line. The discovery of *MyoD* was a turning point in myogenesis research [12] and the *MyoD* gene family is now believed to control the major path of myogenesis [13].

Adipogenesis was also investigated using the same cell line, and *peroxisome proliferator-activated receptor gamma (PPAR gamma)*, a receptor of prostaglandin, was demonstrated to control the adipogenesis [14]. Compared with these investigations of myogenesis, little is known about osteogenesis and chondrogenesis. In 1997, a member of the RUNX family, CBFA1 (RUNX2) was demonstrated to be involved in osteogenesis, in a study of a null mutant mouse [15]. Recently, a type of zinc finger protein, called "osterix", was also reported to be involved in osteogenesis [16]. But the commitment of these transcriptional factors was not enough to initiate osteogenesis. Some other factors seem to be involved, but systematic investigation has not yet been done. One of the reasons might be that the cells used for such studies, e.g., primary cultures of osteoblasts or osteosarcoma cell lines, had inadequate capacity for bone formation [17,18].

Umezawa et al. [6] in experiments attempting the immortalization of murine bone marrow stromal cells, succeeded in the establishment of several mesenchymal progenitor cell lines (KUMs). One of them, named "Kusa", was unique in that it had osteogenesis potential in vivo. We investigated this cell line from the molecular aspect, including the use of cDNA microarray, to analyze the global dynamics of its gene expression pattern (gene profiling) [1,19].

Materials and methods

Cell culture

Kusa was established from mouse bone marrow stromal cells. Briefly, eluted stromal cells from the femoral bone marrow were transferred to a Dexter-type long-term culture [6]. Limiting dilution and continuous passage were performed to isolate the monoclonal cell populations. Various types of cell line were identified (KUMs) and one of them, named "Kusa", was found to possess osteoblastic properties in vivo. Five independent sublines were established from the in vivo cell mass of Kusa, after in vitro culture with limiting dilution. One of them, Kusa-A1, was selected for its particularly high osteogenic activity, and another subline, Kusa-O, was identified as non-osteogenic, although it had high alkaline phosphatase (ALP) activity. Kusa-A1 and Kusa-O were cultured in α-modified minimum essential medium containing 10% fetal calf serum. Cells were inoculated at 5000 cells/cm^2 and incubated until confluency for passage. Mineralization was induced by adding 0.2 mM ascorbic acid and 5 mM β-glycerophosphate to the same medium after confluency (inducing condition) [20,21].

Measurement of alkaline phosphatase (ALP) activity and calcium content

Alkaline phosphatase (ALP) activity was measured with an ALP measurement kit, (ALP-K Test, Wako Chemicals, Tokyo, Japan). The accumulation of calcium deposits was measured with a calcium measuring kit, Ca-E Test (Wako Chemicals), using the cell extracts treated with HCl. To determine these two activities in the cell population, normalization was performed by measuring the protein concentration in extracts. The protein concentration was measured with a DC Protein assay kit (Bio-Rad, Hercules, CA, USA). All measurements were performed by independent triplicate studies.

Northern blot and reverse transcription-quantitative reverse transcription (RT)-quantitative polymerase chain reaction (qPCR) analysis

Total RNA was extracted and purified with TRIzol (Invitrogen, Carlsbad, CA, USA). Ten micrograms of total RNA was applied to each lane of 1.2% formaldehyde agarose gel and electrophoresed. The RNA was transferred to a Nylon membrane (HybondN+; Amersham Biosciences, Piscataway, NJ, USA) and hybridized to ^{32}P-labeled DNA probes. Signals were detected and measured with a digital image analyzer, BAS-2500 (Fuji Photo Film, Tokyo, Japan). Labeled cDNA probes were made using a 488-bp fragment of mouse *Osteocalcin* (*OC*) cDNA (provided by J. Wozney [Celeste et al. [22]), a 984-bp fragment of mouse *Osteopontin* (*OPN*) cDNA (provided by Nomura et al. [23]), a 2673-bp fragment of mouse *Notch1* intracellular domain cDNA (provided by J. Nye), a 1609-bp fragment of rat *HES1* cDNA (provided by R. Kageyama), and a 2380-bp fragment of mouse *CCN3 nephroblastoma overexpressed gene (Nov)*, cloned by B. Perbal. The qPCR was performed (DyNAmo, DNA engine Opticon; MJ Japan, Tokyo, Japan) with the first-strand cDNA synthesized from 500 ng of total RNA (SuperScript II; Invitrogen). The primer sequences were as follows: MEF2C (141 bp): 5′-ATGGA TGAGCGTAACAGACAGGTG-3′ and 5′-CGTTGTAC TCGGTGTACTTGAGCA-3′; periostin (100 bp): 5′-ACC CTGCAAATGCCAACAGT-3′ and 5′-AGAATTTGCT GGAGGGCACA-3′; and βactin (380 bp): 5′-TCGGTCA GGATCTTCATGAG-3′ and 5′-AGTACCCCATTGAA CATGGC-3′.

cDNA array analysis

Global examination of gene expression was performed with a cDNA gene expression array (Atlas mouse cDNA Expression Array; BD Biosciences Clontech, Palo Alto, CA, USA). This microarray carries 588 mouse cDNAs for general profiling. The complete list of cDNAs is available at the website of Clontech (http://www.clontech.com). The extracted total RNA was eluted through an oligo-dT cellulose (Amersham Sciences, Piscataway, NJ, USA) column to purify polyA mRNA. cDNA probes were made from the poly A mRNA, following the manufacturer's protocol, with the specific primers and [α-^{32}P] dATP and hybridized to the array membrane. Signals were detected and measured with a digital image analyzer (BAS-2500).

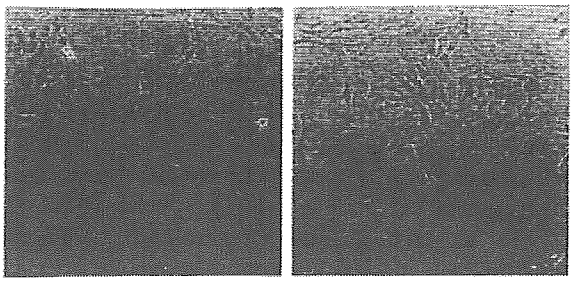

Fig. 1. Phase contact photomicrographs of Kusa-A1 and Kusa-O. Morphologically, Kusa-A1 (**A**) and Kusa-O (**B**) were similar, with a spindle or polygonal shape. Kusa-O was slightly larger than Kusa-A1 in cell size. *Bar* represents 100 μm

Another microarray analysis was done with the GEMarray (Incyte/Genome Systems, Palo Alto, CA, USA). This microarray was based on a fluorescence labeled (Cy3 and Cy5) cDNA probe to distinguish the two sources. Hybridization on the slide glasses and image analysis were done by the company. The results were expressed in reference to the GenBank addresses.

Results

Morphological properties of Kusa

Before confluence, Kusa-A1 had a fibroblastic appearance, with a polygonal flat or spindle shape (Fig. 1A). Kusa-O was slightly larger than Kusa-A1 in cell size (Fig. 1B), although no significant difference was observed. Kusa did not exhibit tumor-cell-like growth, such as piling up, nor did it form a focus in normal medium (non-inducing condition). On treatment with ascorbic acid and β-glycerophosphate (inducing condition), Kusa-A1 exhibited mineralization (Fig. 2). Kusa-A1 gradually accumulated extracellular matrices as small sandy precipitates that covered the surface of cell aggregates. The accumulation was positively stained with Alizarin Red S. These nodules were visible on day 3 and showed condensed staining on day 5 (Fig. 2B,C). In the non-inducing condition, Kusa-A1 spontaneously exhibited nodule-like structures on day 5, although the nodules were rather small and not stained with Alizarin Red S (Fig. 2A). Kusa-O did not exhibit rapid mineralization. In the inducing condition, mineralized nodules were gradually accumulated from day 10 (Fig. 2E,F,G). The Alizarin Red S-positive spots in Kusa-O were rather large but diffuse, and their margins were not clear, as compared with the nodule margins in Kusa-A1. In the non-inducing condition, Kusa-O formed nodules, but they were rather small and not stained with Alizarin Red S (Fig. 2D). High magnification of the Kusa-A1 culture stained with Alizarin Red S showed that the calcified area appeared like "spots", distinctly separate from the non-calcified area (Fig. 2H). The calcified area in Kusa-O showed obscure margins and non-condensed stain (Fig. 2I).

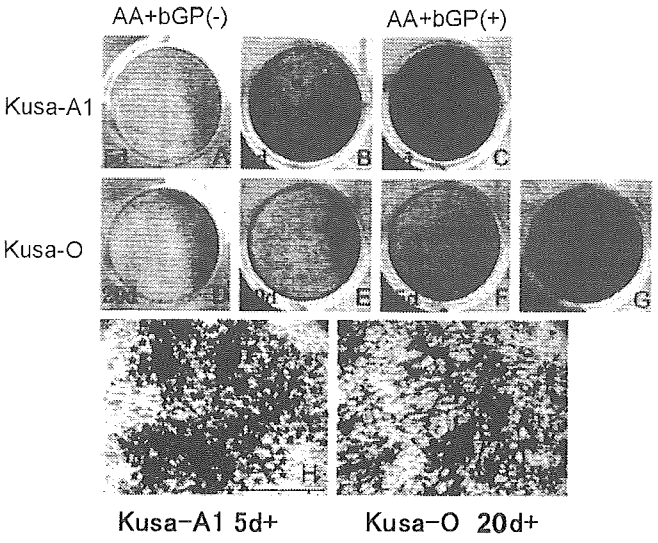

Fig. 2. Mineralized nodule formation in *Kusa-A1* and *Kusa-O*. Mineralized nodules were detected by Alizarin Red S staining. Kusa-A1 cultured in the non-inducing condition (without ascorbic acid [*AA*] and β-glycerophosphate [*βGP; AA* + *βGP*(−)] did not form mineralized nodules 5 days (*d*) after confluency (**A**), but in the inducing condition (addition of AA and *βGP AA* + *βGP*(+)) these nodules were formed on day 3 (**B**), and nodules showing condensed staining were formed on day 5 (**C**). Kusa-O did not form mineralized nodules 20 days after confluency in the non-inducing condition (**D**), but, in the inducing condition, formed them on day 10 (**E**); the nodules then developed moderately (**F** day 15; **G** day 20). **H** and **I** show high-magnification views of mineralized nodules. **H** In Kusa-A1, the nodules had a discrete margin (*asterisks* indicating the development of "salt-and-pepper pattern"-like dot structures, but in Kusa-O (**I**), the margins of the nodules were ambiguous. *Bar* represents 500 μm. **A–G** ×1

Calcium accumulation

Kusa-A1 and Kusa-O apparently differed in calcium accumulation rates (Fig. 3). In the non-inducing condition, neither Kusa-A1 nor Kusa-O exhibited calcium accumulation until day 5. However, Kusa-A1 showed marked accumulation of calcium deposits in the inducing condition. On day 5, the calcium level was 20-fold higher than that in the initial state. Kusa-O was not reactive to the inducing condition and showed little change even on day 5. MC3T3-E1 cells (a mouse osteoblastic cell line) did not show apparent accumulation of calcium deposits during the time course.

ALP activity and insoluble calcium content

Kusa-A1 had extraordinarily high ALP activity (0.8 IU/mg) even before mineralization, and this activity was constant both in the inducing and the non-inducing conditions (Fig. 3). The very high ALP activity of Kusa-A1 was marked as compared with that in MC3T3-E1, which had 20-fold less ALP activity than Kusa-A1. Kusa-O had relatively low ALP activity at the beginning (though it was much higher than that in MC3T3-E1), but the activity gradually increased in the inducing condition, to 1.2 IU/mg on day 5.

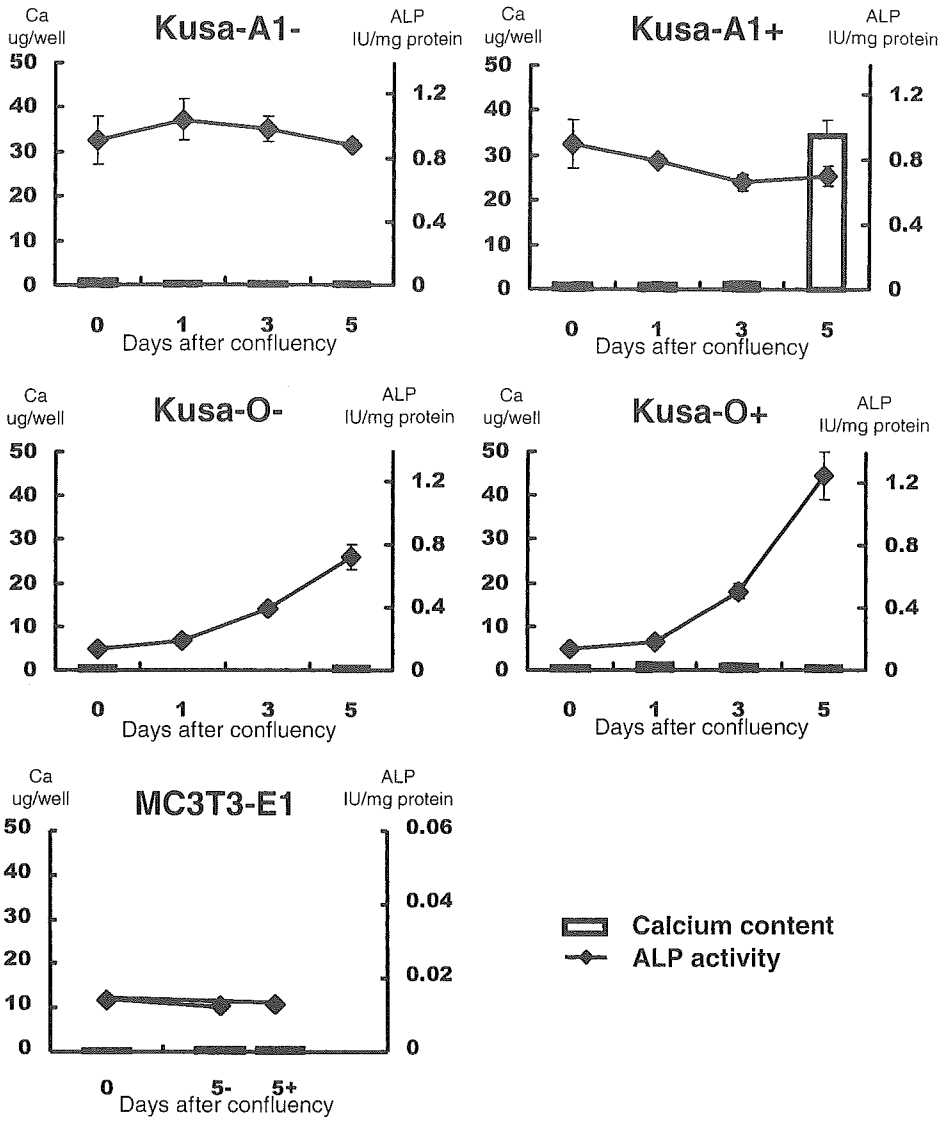

Fig. 3. Calcium accumulation and alkaline phosphatase (*ALP*) activity in Kusa-A1 and Kusa-O Calcium accumulation was observed only in Kusa-A1 on day 5 after confluency in the inducing condition (*Kusa-A1+*). High ALP activity was observed in Kusa-A1 in the non-inducing condition (*Kusa-A1−*) and ALP was rather low in the inducing condition (Kusa-A1+). ALP activity in Kusa-O was not high at the beginning, but was gradually upregulated during the time course in the non-inducing condition (*Kusa-O−*) and the inducing condition accelerated this upregulation (*Kusa-O+*). ALP activity in *MC3T3-E1* was much lower than that in Kusa-A1 and Kusa-O. MC3T3-E1 was cultured in both inducing and non-inducing conditions. *Minus sign* "−" indicates the absence of AA and βGP and "+" indicates the presence of AA and βGP

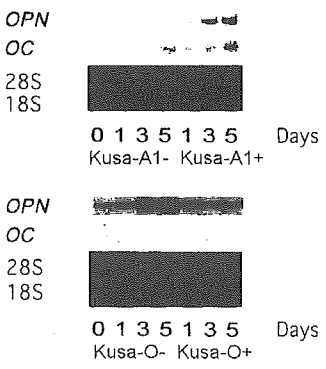

Fig. 4. *Osteocalcin* (*OC*) and Osteopontin (*OPN*) expression in Kusa-A1 and Kusa-O. In Kusa-A1, *Osteocalcin* expression was observed on day 5 in the non-inducing condition, and was seen on day 1 in the inducing condition. Its expression was gradually upregulated in the time course. In contrast, Kusa-O did not express *Osteocalcin*. *Osteopontin* expression was high only in the inducing condition in Kusa-A1, but its expression was observed in both conditions in Kusa-O. *Minus sign* "(−)" indicates the absence of AA and βGP and + indicates the presence of AA and βGP

Expression of osteogenic marker genes

We examined two osteogenic markers, *osteopontin* (*OPN*) and *osteocalcin* (*OC*) (Fig. 4). In Kusa-A1, *osteopontin* expression was not detectable in the non-inducing condition, although *Osteocalcin* was slightly upregulated. In the inducing condition, *osteocalcin* expression was high from day 1 and gradually increased. *Osteopontin* expression was gradually upregulated in the inducing condition. Kusa-O showed a relatively constant level of *osteopontin* expression in the inducing condition, whereas the level was high in the non-inducing condition. *Osteocalcin* expression was not detectable in Kusa-O in either the inducing or the non-inducing condition.

Expression of Notch signal genes

To examine the properties of Kusa as stem cells, genes related to the Notch signal were investigated (Fig. 5). The

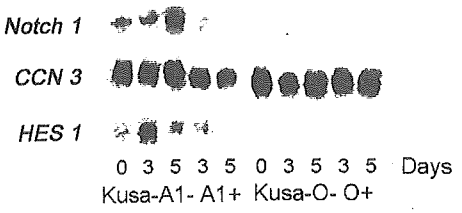

Fig. 5. Notch signal expression in *Kusa-A1* and *Kusa-O*. *Top row*, *Notch1*; *middle row*, *CCN3 (Nov)*; *bottom row*, *HES1*. *Minus sign* (−) indicates the absence of AA and βGP and + indicates the presence of AA and βGP

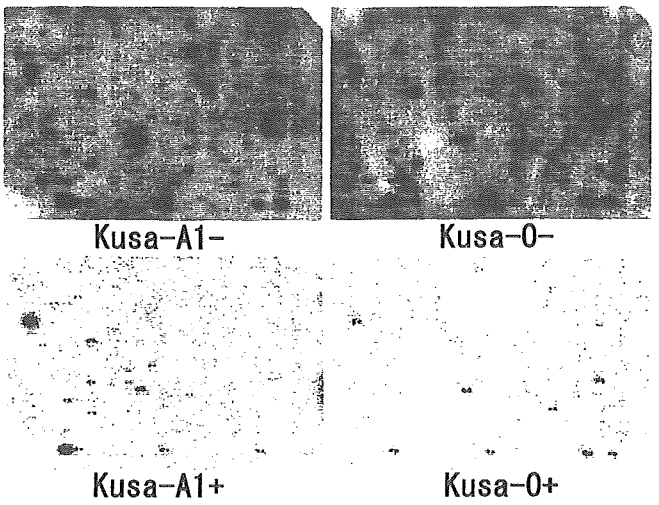

Fig. 6. Atlas Microarray (Clontech) surveillance of Kusa-A1 and Kusa-O in both the non-inducing and the inducing conditions. The profile of Kusa-A1 was generally similar to that of Kusa-O. The inducing condition showed a marked downregulation of gene expression in both cell lines. *Minus sign* (−) indicates the absence of AA and βGP and + indicates the presence of AA and βGP

Notch signal is fundamental for the regulation of stem cells, and *CCN3* is a regulator of the Notch signal whose expression is often found in mesenchymal cells. *CCN3* expression was discrete in both Kusa-A1 and Kusa-O. In Kusa-A1, it was high in the non-inducing condition. *Notch1* expression in Kusa-A1 was observed in the non-inducing condition. Weak *Notch1* expression was observed on day 3 in the inducing condition in both Kusa-A1 and Kusa-O. *HES1* expression in Kusa-A1 was transiently upregulated in the non-inducing condition. In Kusa-O, *HES1* expression was not observed. In conclusion, subtle differences were observed in the expression patterns of the examined genes related to the Notch signal.

Gene expression profile, using cDNA microarray

To clarify the differences in gene expression in Kusa-A1 and Kusa-O in detail, global examination was done using microarray methods. We performed cDNA array analysis of 588 genes with the Atlas Mouse cDNA Expression Array (Clontech) (Fig. 6) in both the inducing and non-inducing conditions. From an overview of the hybridization image, it was clear that global downregulation occurred in the inducing condition in both Kusa-A1 and Kusa-O. In the non-inducing condition, about 140 genes were expressed in the panel, and in the inducing condition, about 50 genes (including several housekeeping genes) were expressed. In about 50 remaining genes, no genes directly involved in osteogenesis were found (Table 1). However, several genes possibly related to osteogenesis (Table 1) showed differences between the cell lines. For Kusa-A1, *ski* and *TIMP 2* and *3* were upregulated in the inducing condition. In contrast, *MAPKK1* and *TGFβ2* were upregulated for Kusa-O.

To compare the expression patterns between Kusa-A1 and Kusa-O, another type of microarray, (GEMarray; Incite/Genome Systems) was carried out, which could analyze more than 8000 clones. Several genes (clones) that showed great differences in expression were demonstrated (Tables 2 and 3) though they did not include known genes directly related to osteogenesis. Tables 2 and 3 show that *myocyte enhancer factor 2C (MEF2C)* is a gene that was highly expressed in Kusa-A1. This gene is regulated principally by other myogenic transcriptional factors, such as MyoD and Myf5, but the GEMarray analysis did not show upregulation of any other myogenic markers. The expression rate of *MEF2C* was also confirmed by qRT-PCR (Fig. 7). In contrast to the expression of *MEF2C* in Kusa-O, *periostin* (also known as *osteblast-specific factor-2 [OSF-2]*) was high in Kusa-O (Fig. 7). The role of this fasciclin 1-like extracellular protein has not yet been clarified, but it may play a role in the recruitment and attachment of osteoblast precursors in the periosteum [24].

Discussion

We investigated the properties of an osteogenic cell line, Kusa, from several aspects. This cell line has unidirectional potential for osteogenesis/mineralization in the normal condition and was classified into two sublines, Kusa-A1 and Kusa-O, by mineralization activity. Kusa-A1 had high ability for osteogenesis/mineralization in vivo and in vitro. The osteogenic ability of Kusa-A1 was remarkable; it showed mineralization within 5 days in the inducing condition, whereas a well-known mouse osteoblastic cell line, MC3T3-E1, first demonstrated mineralized nodules only on day 20 (personal data). Kusa-O was relatively slow to show mineralization as compared with Kusa-A1, but it is not appropriate to call it "non-osteogenic", because its activity was almost the same as that of MC3T3-E1. Both Kusa sublines should be categorized as high osteogenic cell lines.

The high ALP activity of Kusa was remarkable when compared with that of the osteogenic cell line MC3T3-E1. The constant high ALP activity in Kusa-A1 may have influenced its strong mineralization ability, and the progressive upregulation of ALP in Kusa-O would explain its slow mineralization. Calcium deposition was faster in Kusa-A1 than in Kusa-O in the inducing condition, but in the